

EGGS: Eigen-Gap Guided Search Making Subspace Clustering Easy

Jicong Fan, Yiheng Tu, Zhao Zhang, Mingbo Zhao

arXiv:2107.12183v2 [cs.LG] 27 Jul 2021

Abstract—The performance of spectral clustering heavily relies on the quality of affinity matrix. A variety of affinity-matrix-construction methods have been proposed but they have hyper-parameters to determine beforehand, which requires strong experience and lead to difficulty in real applications especially when the inter-cluster similarity is high or/and the dataset is large. On the other hand, we often have to determine to use a linear model or a nonlinear model, which still depends on experience. To solve these two problems, in this paper, we present an eigen-gap guided search method for subspace clustering. The main idea is to find the most reliable affinity matrix among a set of candidates constructed by linear and kernel regressions, where the reliability is quantified by the *relative-eigen-gap* of graph Laplacian defined in this paper. We show, theoretically and numerically, that the Laplacian matrix with a larger relative-eigen-gap often yields a higher clustering accuracy and stability. Our method is able to automatically search the best model and hyper-parameters in a pre-defined space. The search space is very easy to determine and can be arbitrarily large, though a relatively compact search space can reduce the highly unnecessary computation. Our method has high flexibility and convenience in real applications, and also has low computational cost because the affinity matrix is not computed by iterative optimization. We extend the method to large-scale datasets such as MNIST, on which the time cost is less than 90s and the clustering accuracy is state-of-the-art. Extensive experiments of natural image clustering show that our method is more stable, accurate, and efficient than baseline methods.

Index Terms—subspace clustering, model and hyper-parameter search, relative eigen-gap, large-scale clustering

I. INTRODUCTION

Clustering is an unsupervised machine learning problem and plays important roles in many areas such as computer science, biology, and social science. The best-known clustering method is the k-means clustering that enjoys extensive applications owing to the high simplicity and efficiency of algorithm implementation. One limitation of k-means clustering is that it is not effective in handling data lying in a union of subspaces, where the data distribution is not in the format of clusters characterized by cluster centres and Euclidean distance. To solve this problem, in the past decade, numerous subspace clustering methods have been proposed [39]. Subspace clustering has two key procedures: 1) construct or learn an affinity matrix that captures the similarity between pair-wise data points; 2) perform spectral clustering [40] that computes the first k

Jicong Fan is with the School of Data Science, The Chinese University of Hong Kong, Shenzhen, China. Yiheng Tu is with The Chinese Academy of Science, China. Zhao Zhang is with the School of Computer Science and Information Engineering, Hefei University of Technology, China. Mingbo Zhao is with the School of Information Science, Donghua University, China. Corresponding author: Jicong Fan. E-mail: fanjicong@cuhk.edu.cn.

eigenvectors of the Laplacian matrix and apply k-means to the k -dimension data formed by the eigenvectors.

The performance of subspace clustering or spectral clustering more generally heavily relies on the quality of affinity matrix. A variety of methods have been proposed to construct or learn affinity matrices. Many of them are in the framework of self-expressive [5] model

$$\underset{\mathbf{C}}{\text{minimize}} \quad \frac{1}{2} \|\mathbf{X} - \mathbf{X}\mathbf{C}\|_F^2 + \lambda \mathcal{R}(\mathbf{C}). \quad (1)$$

Here the columns of $\mathbf{X} \in \mathbb{R}^{m \times n}$ are the data points drawn from a union of subspaces; $\mathbf{C} \in \mathbb{R}^{n \times n}$ is a coefficient matrix; $\mathcal{R}(\mathbf{C})$ denotes a regularization operator on \mathbf{C} ; λ is a hyper-parameter to be determined in advance. In [5], Elhamifar and Vidal utilized $\mathcal{R}(\mathbf{C}) = \|\mathbf{C}\|_1 := \sum_{i=1}^n \sum_{j=1}^n |c_{ij}|$ and let $\text{diag}(\mathbf{C}) = \mathbf{0}$. Since $\|\cdot\|_1$ is a convex surrogate of the number of nonzero elements of matrix, the \mathbf{C} in (1) is encouraged to be sparse. In [5], the affinity matrix for spectral clustering is given by $\mathbf{A} = |\mathbf{C}| + |\mathbf{C}|^\top$. Theoretically, if \mathbf{x}_i and \mathbf{x}_j are from different subspaces, a_{ij} should be zero. The method is called Sparse Subspace Clustering (SSC). By slightly modifying (1), SSC can handle sparse noise and outliers [5].

Following the self-expressive framework (1), Liu et al. [21] let $\mathcal{R}(\mathbf{C}) = \|\mathbf{C}\|_*$ and proposed a Low-Rank Representation (LRR) method for subspace clustering. Here $\|\mathbf{C}\|_*$ denotes the nuclear norm of \mathbf{C} defined as the sum of singular values and is a convex surrogate of matrix rank function. They considered an additional \mathbf{E} penalized by $\ell_{2,1}$ norm (sum of ℓ_2 norms of the columns of matrix, a convex relaxation of the number of nonzero columns). Thus, LRR encourages \mathbf{C} to be low-rank to recognize the low-dimensional structure of the data and encourages \mathbf{E} to be column-wise sparse to recognize the outliers in \mathbf{X} .

Lu et al. [23] showed that, similar to SSC and LRR, the least squares regression (LSR) model, (1) with $\mathcal{R}(\mathbf{C}) = \|\mathbf{C}\|_F^2$, is also able to identify the subspaces of \mathbf{X} . Ji et al. [29] provided a robust version of LSR called EDSC for subspace clustering. Compared to SSC and LRR, LSR has much lower computational cost because the \mathbf{C} has a closed-form solution [23]. A few variants of LRR and SSC can be found in [31], [17], [30], [36], [18]. Recently, deep learning based subspace clustering methods [11], [47], [46], [35], [13] have achieved state-of-the-art performance on many benchmark datasets. We will not detail them in this paper.

One common limitation of the aforementioned methods is that they are not scalable to large-scale datasets. The first reason is that the time complexity of learning an affinity matrix based on the self-expressive model is often $O(n^2)$ or even $O(n^3)$ in every iteration of the optimization and the space

complexity is $O(n^2)$ in many cases. The second reason is that the eigenvalue decomposition of the Laplacian matrix has polynomial time complexity.

Another common limitation of those methods is that they have at least¹ one hyper parameter (e.g. “ λ ”) to determine in advance. Since subspace clustering is an unsupervised learning problem, the hyper parameters cannot be tuned by cross validation that is widely used in supervised learning. Thus, we have to tune the hyper parameters in subspace clustering by experience, which is difficult when the given dataset is quite different from those in our experience or/and the inter-class similarity is high compared to the intra-cluster similarity. Moreover, when the dataset is large, hyper-parameter tuning will cost too much time.

This paper aims at the aforementioned two limitations of subspace clustering. Our contributions are three-fold.

- We propose an eigen-gap guided search method called EGGS for subspace clustering. The method finds the Laplacian matrix with largest *relative-eigen-gap* among a set of candidates constructed by linear or kernel regressions with different penalty parameters followed by different truncations. The search space of the proposed method is very easy to determine and can be arbitrarily large. In addition, the method has low computational cost because there is no iterative optimization when constructing affinity matrices.
- To cluster large-scale data, we propose to apply EGGS to a set of landmarks of the dataset. We then use neural network to learn a nonlinear mapping from the landmarks to the nullspace of the Laplacian matrix given by EGGS. The nonlinear mapping is used to encode the whole data into a cluster-informative low-dimensional space, in which k-means is performed to find the clusters.
- We provide theoretical analysis for the effectiveness of the proposed methods.

We test EGGS on a few benchmark image datasets and show that EGGS is more flexible and efficient than many baselines. EGGS also has higher clustering accuracy than the baselines in many cases. In addition, the large-scale extension of EGGS is able to outperform state-of-the-art methods of large-scale subspace clustering.

II. RELATED WORK

A. Large-scale subspace clustering

A few researchers have developed large-scale subspace clustering methods [3], [33], [2], [41], [32], [44], [45], [20], [43], [19], [4], [12]. For instance, Cai and Chen [2] proposed a landmark-based spectral clustering (LSC) that selects a few landmark points to represent the original data points linearly, by which the spectral embedding can be efficiently computed for clustering. Peng et al. [33], [32] proposed to perform SSC on a few landmark data points to build a classifier, which is used to classify the other data points. In contrast to [2], [33], [32] that taking advantage of landmark points, You et

¹In the codes of SSC and its variants provided by the authors of the corresponding papers, there is usually a thresholding parameter for the affinity matrix, which influences the clustering accuracy a lot.

al [45] proposed to learn the sparse coefficient matrix of SSC by orthogonal matching pursuit (OMP), which greatly reduced the space and time complexity of SSC. Shin and Maria [25] presented a method called S⁵C that performs subset section via sparse representation iteratively and then represents all data points by the subset to construct an affinity matrix for spectral clustering. There is still a lot of room to improve the accuracy, efficiency, and convenience (e.g. hyper-parameter tuning) of these methods.

B. Exploit eigenvalue information for clustering

It is known that the number of zero eigenvalues of a Laplacian matrix is equal to the number of connected components of the graph [40]. Hence a few researchers have considered to learn a Laplacian matrix of which the k smallest eigenvalues are as small as possible [27]. For instance, Ji et al. [10] utilized eigen-gap to determine the rank of the Shape Interaction Matrix. They constructed a few affinity matrices by $\mathbf{A}_r = [\tilde{\mathbf{V}}_r \tilde{\mathbf{V}}_r^\top]^{\odot \gamma}$ where $\tilde{\mathbf{V}}_r$ is composed of the row-normalized first r right singular vectors of \mathbf{X} . Then the affinity matrix \mathbf{A}_{r^*} was used for spectral clustering, where

$$r^* = \underset{r \in [r_{\min}, r_{\max}]}{\operatorname{argmin}} \frac{\text{minCut}(\mathbf{A}_r^{(1)}, \dots, \mathbf{A}_r^{(k)})}{\sigma_{k+1}(\mathbf{L}) - \sigma_k(\mathbf{L})}, \quad (2)$$

and $\sigma_k(\mathbf{L})$ denotes the k -th eigenvalue of the Laplacian matrix \mathbf{L} . Hu et al. [9] proposed to learn a weight vector for the features to maximize the eigen-gap of Laplacian matrix:

$$\underset{\mathbf{w} \in \Delta^m}{\operatorname{maximize}} \sigma_{k+1}(\mathbf{L}) - \sigma_k(\mathbf{L}), \quad (3)$$

where Δ^m denotes a m -simplex and $\sigma_k(\mathbf{L})$ denotes the k -th eigenvalue of the Laplacian matrix \mathbf{L} . \mathbf{L} is constructed from $S_{ij} = \exp(-\|\mathbf{x}'_i - \mathbf{x}'_j\|^2)$, where $\mathbf{x}' = \mathbf{w} \odot \mathbf{x}$. [9]. Lu et al. [22] showed SSC is related to the following problem

$$\underset{\mathbf{Z}, \mathbf{B}}{\operatorname{maximize}} \frac{1}{2} \|\mathbf{X} - \mathbf{XZ}\|_F^2 + \frac{\lambda}{2} \|\mathbf{Z} - \mathbf{B}\|_F^2 + \gamma \|\mathbf{B}\|_{[k]}, \\ \text{subject to } \operatorname{diag}(\mathbf{B}) = \mathbf{0}, \mathbf{B} \geq \mathbf{0}, \mathbf{B} = \mathbf{B}^\top, \quad (4)$$

where $\|\mathbf{B}\|_{[k]} = \sum_{i=1}^k \sigma_i(\mathbf{L}_B)$ and $\mathbf{L}_B = \operatorname{diag}(\mathbf{B} \mathbf{1}) - \mathbf{B}$. Solving (4) will minimize the smallest k eigenvalues of the Laplacian matrix while controlling the self-expressive error.

The method of [10] requires to determine γ beforehand and needs to perform spectral clustering for multiple times. The methods of [27], [9], [22] are based on iterative optimization (need to perform eigenvalue decomposition at every iteration) and hence are not effective in handling large-scale datasets. In addition, although the BDR method of [22] showed higher clustering accuracy than SSC, LRR, and LSR on a few benchmark datasets, tuning the two hyper parameters, say λ and γ , requires domain expert or strong experience, which yields inconvenience in real applications.

Figure 1 shows the clustering accuracy of SSC [5], LRR [21], and BDR-B [22] with different hyper parameters and our method EGGS on the Extended Yale Face B subset [15]. We see that SSC and BDR-B are sensitive to the value of λ , especially for the relatively difficult task, say Figure 1(b). LRR is not sensitive to the value of λ but its accuracy is low. EGGS is more accurate and efficient than other methods.

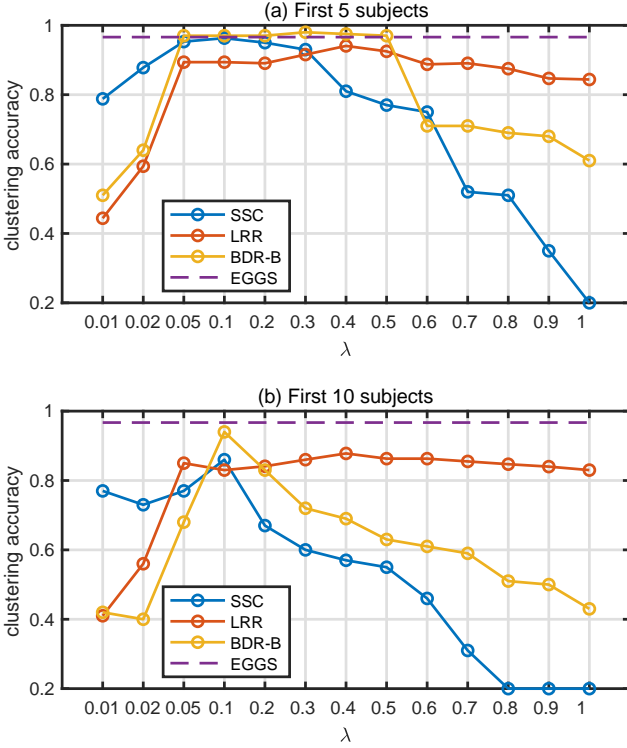


Fig. 1. Clustering accuracies of SSC, LRR, and BDR-B (4) with different hyper parameter λ on the Extended Yale Face B database. The value of λ used in BDR-B has been divided by 10. The γ in BDR-B is chosen from $\{0.01, 0.1, 1\}$ and the best one is used for each λ . In Case (b), the time costs of SSC, LRR, BDR-B, and EGGS are 9.5s, 33.0s, 7.6s, and 1.6s respectively.

III. EGGS FOR SUBSPACE CLUSTERING

A. Preliminary Knowledge

Let $\mathbf{A} \in \mathbb{R}^{n \times n}$ be an affinity matrix constructed from a given a data matrix $\mathbf{X} \in \mathbb{R}^{m \times n}$. The corresponding graph is denoted by $G = (V, E)$, where $V = \{v_1, \dots, v_n\}$ is the vertex set and $E = \{e_1, \dots, e_l\}$ is the edge set. The degree matrix of a graph G is defined as $\mathbf{D} = \text{diag}(\mathbf{A}\mathbf{1})$, where $\mathbf{1} = [1, 1, \dots, 1]^\top$. Our goal is to partition the vertices in to k disjoint nonempty subsets C_1, \dots, C_k . Let $\mathcal{C} = \{C_1, \dots, C_k\}$. It is expected to find a partition \mathcal{C} that minimizes the following metric:

Definition 1 (MNCut). *The multiway normalized cut (MNCut) [26] is defined as*

$$\text{MNCut}(\mathcal{C}) = \sum_{i=1}^k \sum_{j \neq i} \frac{\text{Cut}(C_i, C_j)}{\text{Vol}(C_i)}, \quad (5)$$

where $\text{Cut}(C_i, C_j) = \sum_{u \in C_i} \sum_{v \in C_j} A_{uv}$ and $\text{Vol}(C_i)$ denotes the sum of the vertex degrees of C_i .

The normalized graph Laplacian matrix is defined as

$$\mathbf{L} = \mathbf{I} - \mathbf{D}^{-1/2} \mathbf{A} \mathbf{D}^{-1/2}, \quad (6)$$

where \mathbf{I} is an identity matrix. The normalized graph Laplacian is often more effective than unnormalized one in spectral clustering (some theoretical justification was given by Von Luxburg [40]). Let $\sigma_i(\mathbf{L})$ be the i -th smallest eigenvalue of \mathbf{L} .

The following claim shows the connection between $\text{MNCut}(\mathcal{C})$ and \mathbf{L} .

Claim 1. *The sum of the k smallest singular values of \mathbf{L} quantifies the potential connectivity among C_1, \dots, C_k :*

$$\text{MNCut}(\mathcal{C}) \geq \sum_{i=1}^k \sigma_i(\mathbf{L}). \quad (7)$$

The claim can be easily proved by using Lemma 4 of [26]. We defer all proof in this paper to the supplementary material. The following proposition shows the connection between the multiplicity of the eigenvalue 0 of \mathbf{L} and the number of connected components of G .

Proposition 1 (Proposition 4 in [40]). *Let G be an undirected graph with non-negative weight. Then the multiplicity k of the eigenvalue 0 of \mathbf{L} equals to the number of connected components C_1, \dots, C_k in G . The eigenvector space of 0 is spanned by the vectors $\mathbf{D}^{1/2} \mathbf{1}_{H_i}$, where $\mathbf{1}_{C_i} = [u_1, \dots, u_n]^\top$ is an indicator vector with $u_j = 1$ if $j \in C_i$ and $u_j = 0$ otherwise.*

Hence we expect to construct an affinity matrix \mathbf{A} from \mathbf{X} such that \mathbf{L} has k zero eigenvalues. Thus the optimal partition means $\text{MNCut}(\mathcal{C}) = \sum_{i=1}^k \sigma_i(\mathbf{L}) = 0$.

B. Eigen-Gap Guided Search

In practice, we may construct an \mathbf{A} such that² $\sum_{i=1}^k \sigma_i(\mathbf{L})$ is as small as possible because guaranteeing zero eigenvalues is difficult. However, this is not enough because the \mathbf{L} of a candidate \mathbf{A} may have $k+1$ or more very small or even zero eigenvalues.

It is known that the second smallest eigenvalue of the Laplacian matrix of a graph G is called the algebraic connectivity of G (denoted by $ac(G)$) [6]. We have $ac(G) = 0$ if and only if G is not connected. When G has k disjointed components, there are k algebraic connectivities, denoted by $ac(C_1), \dots, ac(C_k)$. Then $\sigma_{k+1}(\mathbf{L}) = \min_{1 \leq i \leq k} ac(C_i)$ if $\sigma_1(\mathbf{L}) = \dots = \sigma_k(\mathbf{L}) = 0$. We have

Claim 2. *The $k+1^{th}$ smallest eigenvalue of \mathbf{L} quantifies the least potential connectivity of the partitions C_1, \dots, C_k of \mathcal{C} :*

$$\min_{1 \leq i \leq k} \text{MNCut}(C_i) \geq \sigma_{k+1}(\mathbf{L}). \quad (8)$$

In other words, $\sigma_{k+1}(\mathbf{L})$ measures the difficulty in segmenting each of C_i into two subsets. Hence, when $\sigma_{k+1}(\mathbf{L})$ is large, the partitions C_1, \dots, C_k are stable. Based on Claim 1 and Claim 2, we may construct an \mathbf{A} that has small $\sum_{i=1}^k \sigma_i(\mathbf{L})$ and large $\sigma_{k+1}(\mathbf{L})$ simultaneously, by solving

$$\begin{aligned} & \underset{\theta}{\text{maximize}} \quad \sigma_{k+1}(\mathbf{L}) - \frac{1}{k} \sum_{i=1}^k \sigma_i(\mathbf{L}), \\ & \text{subject to} \quad \mathbf{L} = \mathbf{I} - \mathbf{D}^{-1/2} \mathbf{A} \mathbf{D}^{-1/2}, \quad \mathbf{A} = f_{\theta}(\mathbf{X}), \end{aligned} \quad (9)$$

²We may also want to ensure that the first k eigenvectors are sparse, which however is difficult to guarantee.

where f_θ denotes a function with parameter θ . We have many choices for f . For instance, when considering the sparse self-expression, f_θ can be implicitly determined by

$$\mathbf{X} = \mathbf{X}\mathbf{C}, \text{ diag}(\mathbf{C}) = \mathbf{0}, \mathbf{A} = |\mathbf{C}| + |\mathbf{C}^\top|, \lambda = \theta. \quad (10)$$

We see that solving (9) directly can be difficult, though one may design an f_θ that is simpler than (10). On the other hand, in (9), we have to choose f in advance, which requires domain expert or strong experience because different dataset usually needs different f . For instance, when one dataset has strong nonlinearity, we may use a nonlinear self-expressive model [31].

Instead of solving (9), we propose to solve

$$\begin{aligned} \underset{f \in \mathcal{F}, \theta \in \Theta}{\text{maximize}} \quad & \frac{\sigma_{k+1}(\mathbf{L}) - \frac{1}{k} \sum_{i=1}^k \sigma_i(\mathbf{L})}{\frac{1}{k} \sum_{i=1}^k \sigma_i(\mathbf{L}) + \epsilon}, \\ \text{subject to} \quad & \mathbf{L} = \mathbf{I} - \mathbf{D}^{-1/2} \mathbf{A} \mathbf{D}^{-1/2}, \mathbf{A} = f_\theta(\mathbf{X}), \end{aligned} \quad (11)$$

where \mathcal{F} is a set of pre-defined functions and Θ is a set of parameters. So (11) is equivalent to choose one \mathbf{A} (or \mathbf{L}) from a sets of candidates constructed by different f with different θ , of which the *relative-eigen-gap*³

$$\text{reg}(\mathbf{L}) := \frac{\sigma_{k+1}(\mathbf{L}) - \frac{1}{k} \sum_{i=1}^k \sigma_i(\mathbf{L})}{\frac{1}{k} \sum_{i=1}^k \sigma_i(\mathbf{L}) + \epsilon} \quad (12)$$

is largest. In $\text{reg}(\mathbf{L})$, the denominator is used to normalize the small eigenvalues because the scale of the small eigenvalues are sensitive to the choice of f and θ . The ϵ in $\text{reg}(\mathbf{L})$ is a small constant such as 10^{-6} to avoid zero denominator.

The following theorem⁴ shows the connection between $\text{reg}(\mathbf{L})$ and the stability of the clustering \mathcal{C} .

Theorem 1. *Let \mathcal{C} and \mathcal{C}' be two partitions of the vertices of G , where $|\mathcal{C}| = |\mathcal{C}'| = k$. Define the distance between \mathcal{C} and \mathcal{C}' as*

$$\text{dist}(\mathcal{C}, \mathcal{C}') = 1 - \frac{1}{k} \sum_{C_i \in \mathcal{C}} \sum_{C'_j \in \mathcal{C}'} \frac{(\text{Vol}(C_i \cap C'_j))^2}{\text{Vol}(C_i) \text{Vol}(C'_j)}. \quad (13)$$

Suppose $\eta k \epsilon \geq \sum_{i=1}^k \sigma_i(\mathbf{L}) \geq k \epsilon$ and $\text{reg}(\mathbf{L}) > (k-1)\eta/2$. Let $\delta = \max(\text{MNCut}(\mathcal{C}) - \sum_{i=1}^k \sigma_i(\mathbf{L}), \text{MNCut}(\mathcal{C}') - \sum_{i=1}^k \sigma_i(\mathbf{L}))$. Then

$$\text{dist}(\mathcal{C}, \mathcal{C}') < \frac{1.5\delta\epsilon^{-1}}{\text{reg}(\mathbf{L}) + (1-k)\eta/2}. \quad (14)$$

It indicates that when $\text{reg}(\mathbf{L})$ is large and δ is small, the partition \mathcal{C} and \mathcal{C}' are close to each other. Thus, the clustering has high stability. When $\sum_{i=1}^k \sigma_i(\mathbf{L}) = k\epsilon$, we have

$$\text{dist}(\mathcal{C}, \mathcal{C}') < \frac{6\delta}{\sigma_{k+1}(\mathbf{L}) - k\epsilon},$$

which means the larger $\sigma_{k+1}(\mathbf{L})$ the more stable clustering.

³Eigen-gap is usually defined as $\sigma_{k+1} - \sigma_k$. In this paper, we use “Eigen-gap” for convenience. On the other hand, σ_k is sensitive to noise and an average of $\sigma_1, \dots, \sigma_k$ is more stable. A comparative study is in Section 2.4 of the supplement.

⁴This theorem is a modified version of Theorem 1 in [27], which is for the eigen-gap $\sigma_{k+1} - \sigma_k$ of \mathbf{L} . Here we consider $\text{reg}(\mathbf{L})$ instead.

C. Regression Search Space

In (11), we have many choices for \mathcal{F} and Θ . For example, when \mathcal{F} is given by SSC, Θ can be a set of values for the λ in (1), e.g. $\Theta = \{0.01, 0.1, 1\}$. Nevertheless, solving (1) requires iterative optimization and hence is not effective when the dataset is large. We propose to solve

$$\underset{\mathbf{C}}{\text{minimize}} \quad \frac{1}{2} \|\mathbf{X} - \mathbf{X}\mathbf{C}\|_F^2 + \frac{\lambda}{2} \|\mathbf{C}\|_F^2, \quad (15)$$

of which the closed-form solution is

$$\mathbf{C} = (\mathbf{X}^\top \mathbf{X} + \lambda \mathbf{I})^{-1} \mathbf{X}^\top \mathbf{X}. \quad (16)$$

Let $\text{diag}(\mathbf{C}) = \mathbf{0}$ and $\mathbf{C} \leftarrow |\mathbf{C}|$, the affinity matrix can be constructed as $\mathbf{A} = (\mathbf{C} + \mathbf{C}^\top)/2$. Lu et al. [23] has shown that the least squares regression (15) is able to identify the subspaces, but determining λ still relies on experience and should be selected from Θ . Another problem is that the off-diagonal elements of \mathbf{A} are dense, which can lead to low clustering accuracy [22]. Therefore, we propose to truncate \mathbf{C} by keeping only the largest τ elements of each column of \mathbf{C} , where τ can be selected from \mathcal{T} . Then the search space we considered is $\Theta \times \mathcal{T}$.

In the case that the data have some low-dimensional nonlinear structures, the similarity between pair-wise columns of \mathbf{X} cannot be well recognized by the linear regression (15). Therefore, we also consider the following nonlinear regression model

$$\underset{\mathbf{C}}{\text{minimize}} \quad \frac{1}{2} \|\phi(\mathbf{X}) - \phi(\mathbf{X})\mathbf{C}\|_F^2 + \frac{\lambda}{2} \|\mathbf{C}\|_F^2, \quad (17)$$

where ϕ denotes a nonlinear feature map performed on each column of the matrix, i.e. $\phi(\mathbf{X}) = [\phi(\mathbf{x}_1), \dots, \phi(\mathbf{x}_n)]$. Letting ϕ be some feature map induced by a kernel function $k(\cdot, \cdot)$, then we reformulate (17) as

$$\underset{\mathbf{C}}{\text{minimize}} \quad \frac{1}{2} \text{Tr}(\mathbf{K} - 2\mathbf{K}\mathbf{C} + \mathbf{C}^\top \mathbf{K}\mathbf{C}) + \frac{\lambda}{2} \|\mathbf{C}\|_F^2, \quad (18)$$

where $\mathbf{K} = \phi(\mathbf{X})^\top \phi(\mathbf{X})$ and $[\mathbf{K}]_{ij} = k(\mathbf{x}_i, \mathbf{x}_j)$. The closed form solution is

$$\mathbf{C} = (\mathbf{K} + \lambda \mathbf{I})^{-1} \mathbf{K}. \quad (19)$$

The post-processing is the same as that for (16). Here we use the Gaussian RBF kernel

$$k(\mathbf{x}_i, \mathbf{x}_j) = \exp(-\|\mathbf{x}_i - \mathbf{x}_j\|^2 / (2\varsigma^2)), \quad (20)$$

where ς controls the smoothness of the kernel. It is known that the feature map ϕ induced by the Gaussian RBF kernel is an infinity-order polynomial. When ς is large, the weight of the higher-degree polynomials are small. When ς is sufficiently large, the Gaussian RBF kernel is equivalent to a linear kernel. Therefore, we propose to use a relatively small ς to identify the high nonlinearity if it exists in the data. The default value is $\varsigma = \frac{1}{n^2} \sum_{ij} \|\mathbf{x}_i - \mathbf{x}_j\|$.

The following proposition shows that (18) is able to organize the elements of \mathbf{C} by the similarity between pairwise columns of \mathbf{X} .

Proposition 2. *Let $\hat{\mathbf{c}}$ be the optimal solution of*

$$\underset{\mathbf{c}}{\text{minimize}} \quad \frac{1}{2} \|\phi(\mathbf{y}) - \phi(\mathbf{X})\mathbf{c}\|_F^2 + \frac{\lambda}{2} \|\mathbf{c}\|_F^2, \quad (21)$$

where ϕ is induced by Gaussian RBF kernel and \mathbf{y} is arbitrary. Then

$$\|\hat{c}_i - \hat{c}_j\| \leq \sqrt{2 - 2 \exp(-\|\mathbf{x}_i - \mathbf{x}_j\|^2/(2\varsigma^2))}. \quad (22)$$

As shown in the proposition, when two data points in \mathbf{X} , e.g. \mathbf{x}_i and \mathbf{x}_j , are close to each other, the corresponding two elements in $\hat{\mathbf{c}}$, e.g. \hat{c}_i and \hat{c}_j , have small difference. Hence (19) utilizes local information to enhance \mathbf{C} .

Now we see that our search space is

$$\mathbb{S} = \mathcal{F} \times \Theta \times \mathcal{T}, \quad (23)$$

where $\mathcal{F} = \{(15), (18)\}$, $\Theta = \{\lambda_1, \lambda_2, \dots\}$, and $\mathcal{T} = \{\tau_1, \tau_2, \dots\}$. The problem we want to solve becomes

$$\underset{s \in \mathbb{S}}{\text{maximize}} \quad \text{reg}(\mathbf{L}_s). \quad (24)$$

The whole algorithm of EGGS is shown in Algorithm 1. When $n \ll m$, using the *push-through identity* [8], we reformulate (16) as

$$\mathbf{C} = \mathbf{X}^\top (\lambda \mathbf{I} + \mathbf{X} \mathbf{X}^\top)^{-1} \mathbf{X} \quad (25)$$

to reduce the computational cost from $O(n^3)$ to $O(mn^2)$. In (19), when n is large (e.g. > 5000), we perform randomized SVD [7] on \mathbf{K} : $\mathbf{K} \approx \mathbf{V}_r \Sigma_r \mathbf{V}_r^\top$. Then we have

$$\mathbf{C} \approx \mathbf{V}_r \Sigma_r^{1/2} (\lambda \mathbf{I} + \Sigma_r)^{-1} \Sigma_r^{1/2} \mathbf{V}_r^\top, \quad (26)$$

where $r = 20k$ works well in practical applications. The time complexity of computing \mathbf{C} is $O(r\tau n + rn^2)$. In Line 11 of Algorithm 1, it is equivalent to compute the largest $k+1$ eigenvalues and eigenvectors of $\mathbf{D}^{-1} \mathbf{A}$, which is sparse. Then the computational cost of Line 11 is $O(k\tau n)$. The total time complexity of Algorithm 1 (excluding Line 18) is

$$O(|\Theta|(mn^2 + r\tau n + rn^2) + 2|\Theta||\mathcal{T}|k\bar{\tau}n),$$

where $\bar{\tau}$ denotes the mean value in \mathcal{T} . The time complexity is at most $O(|\Theta|(mn^2 + |\mathcal{T}|k\bar{\tau}n))$ when when $\tau \leq r \leq m \leq n$. It is worth noting that Algorithm 1 can be easily implemented parallelly, which will reduce the time complexity to $O(\max(m, r)n^2 + k\bar{\tau}n)$. On the contrary, SSC, LRR, and their variants require iterative optimization and hence their time complexity is about $O(tmn^2)$, where t denotes the iteration number and is often larger than 100.

Figure 2 shows an intuitive example of the performance of EGGS in clustering a subset of the Extended Yale B database (detailed in Experiments). We see that: 1) in linear regression or kernel regression, for a fixed λ , the τ with larger $\text{reg}(\mathbf{L})$ provides higher clustering accuracy; 2) in linear regression or kernel regression, for a fixed τ , the λ with higher $\text{reg}(\mathbf{L})$ provides higher clustering accuracy; 3) for a fixed λ and a fixed τ , if the linear regression has a larger $\text{reg}(\mathbf{L})$, its clustering accuracy is higher than that of kernel regression, and vice versa. We conclude from Figure 2 that a larger $\text{reg}(\mathbf{L})$ indeed leads to a higher clustering accuracy, which is in consistent with our theoretical analysis.

Algorithm 1 EGGS

Input: \mathbf{X} , k , \mathcal{F} , Θ , \mathcal{T}

1: Normalize the columns of \mathbf{X} to have unit ℓ_2 norm.
2: **for** f_u in \mathcal{F} **do**
3: **for** λ_i in Θ **do**
4: Construct \mathbf{C} by (16) or (19).
5: **for** τ_j in \mathcal{T} **do**
6: $\mathbf{C} \leftarrow |\mathbf{C} \odot (1 - \mathbf{I})|$.
7: Truncate \mathbf{C} with parameter τ_j .
8: For $j = 1, \dots, n$, let $\mathbf{c}_j \leftarrow \mathbf{c}_j / |\mathbf{c}_j|$.
9: $\mathbf{A} = (\mathbf{C} + \mathbf{C}^\top)/2$.
10: $\mathbf{L} = \mathbf{I} - \mathbf{D}^{-1/2} \mathbf{A} \mathbf{D}^{-1/2}$.
11: Compute $\sigma_1, \dots, \sigma_{k+1}$ and $\mathbf{v}_1, \dots, \mathbf{v}_k$.
12: $\Delta_{u_{ij}} = \text{REG}(\mathbf{L})$, $\mathcal{V}_{u_{ij}} = [\mathbf{v}_1, \dots, \mathbf{v}_k]$.
13: **end for**
14: **end for**
15: **end for**
16: $\mathbf{Z} = \mathcal{V}_{\bar{u}\bar{i}\bar{j}}^\top$, where $\{\bar{u}, \bar{i}, \bar{j}\} = \text{argmax}_{u,i,j} \Delta_{u_{ij}}$.
17: Normalize the columns of \mathbf{Z} to have unit ℓ_2 norm.
18: Perform k-means on \mathbf{Z} .
Output: k clusters: C_1, \dots, C_k .

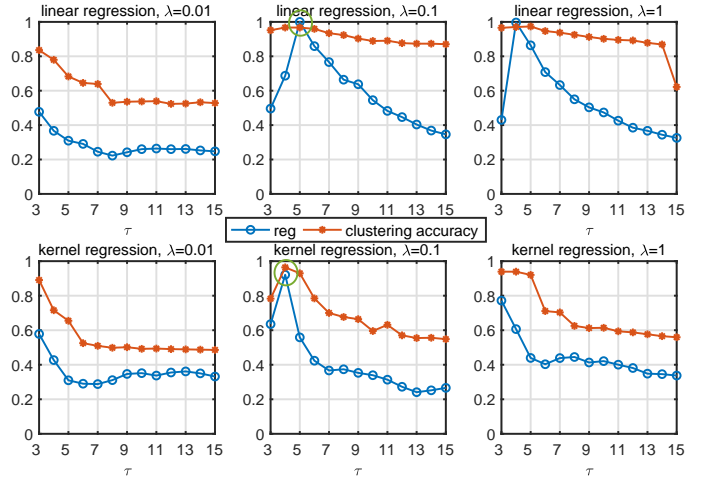


Fig. 2. $\text{reg}(\mathbf{L})$ and clustering accuracy of EGGS on the first 5 subjects of the Extended Yale Face B database [15]. We have scale the $\text{reg}(\mathbf{L})$ into $[0, 1]$ over all cases. The top plots are linear regressions and the bottom plots are kernel regressions.

IV. EGGS+NSE FOR LARGE-SCALE DATA

Since the time and space complexity of EGGS are quadratic with n , it cannot be directly applied to large-scale datasets. To solve the problem, we propose to perform Algorithm 1 on a set of landmarks of the data (denoted by $\hat{\mathbf{X}}$) to get a $\hat{\mathbf{Z}}$. The landmarks can be generated by k-means [3] or randomly. Then we regard $\hat{\mathbf{Z}}$ as a feature matrix and learn a map $g : \mathbb{R}^m \rightarrow \mathbb{R}^k$ from $\hat{\mathbf{X}}$ to $\hat{\mathbf{Z}}$. According to Lines 4-10 and 17 in Algorithm 1, g should be nonlinear and nonsmooth. As proved in [37], a neural network with unbounded activation functions still satisfies the universal approximation property, provided that the number of hidden nodes is sufficiently large. Therefore, we approximate g by a two-layer neural network

and solve

$$\begin{aligned} \underset{\mathbf{W}_1, \mathbf{W}_2, \mathbf{b}_1, \mathbf{b}_2}{\text{minimize}} \quad & \frac{1}{2s} \|\hat{\mathbf{Z}} - \mathbf{W}_2 \text{ReLU}(\mathbf{W}_1 \hat{\mathbf{X}} + \mathbf{b}_1 \mathbf{1}_s^\top) - \mathbf{b}_2 \mathbf{1}_s^\top\|_F^2 \\ & + \frac{\gamma}{2} (\|\mathbf{W}_1\|_F^2 + \|\mathbf{W}_2\|_F^2), \end{aligned} \quad (27)$$

where $\mathbf{W}_1 \in \mathbb{R}^{d \times m}$, $\mathbf{W}_2 \in \mathbb{R}^{k \times d}$, $\mathbf{b}_1 \in \mathbb{R}^d$, and $\mathbf{b}_2 \in \mathbb{R}^k$. Since \mathbf{A} is sparse, k is often less than m , and a neural network is used, we call (27) Neural Sparse Embedding (NSE). We use mini-batch Adam [14] to solve NSE.

When the parameters are estimated, the neural network is applied to the whole data \mathbf{X} to extract a k -dimensional feature matrix \mathbf{Z} :

$$\mathbf{Z} = \hat{g}(\mathbf{X}) = \mathbf{W}_2 \text{ReLU}(\mathbf{W}_1 \mathbf{X} + \mathbf{b}_1 \mathbf{1}_n^\top) + \mathbf{b}_2 \mathbf{1}_n^\top. \quad (28)$$

Finally, we perform k-means on \mathbf{Z} to get the clusters. The procedures are summarized into Algorithm 2. The following proposition shows that a small number of hidden nodes are sufficient to make the clustering succeed.

Proposition 3. Suppose the columns (with unit ℓ_2 norm) of \mathbf{X} are drawn from a union of k independent subspaces of dimension d : $\sum_{j=1}^k \dim(\mathcal{S}_j) = \dim(\mathcal{S}_1 \cup \dots \cup \mathcal{S}_k) = kd$. For $j = 1, \dots, k$, let \mathbf{U}^j be the bases of \mathcal{S}_j and $\mathbf{x}_i = \mathbf{U}^j \mathbf{v}_i$, if $\mathbf{x}_i \in \mathcal{S}_j$. Suppose $\max\{\|\mathbf{U}_{:,l}^i \mathbf{U}^j\| : 1 \leq l \leq d, 1 \leq i \neq j \leq k\} \leq \mu$. Suppose that for all $i = 1, \dots, n$, $\max\{v_{1i}, \dots, v_{di}\} > \mu$. Then there exist $\mathbf{W}_1 \in \mathbb{R}^{d \times m}$, $\mathbf{W}_2 \in \mathbb{R}^{k \times d}$, $\mathbf{b}_1 \in \mathbb{R}^d$, and $\mathbf{b}_2 \in \mathbb{R}^k$ such that performing k-means on \mathbf{Z} will identify the clusters correctly, where $d = kd$.

Algorithm 2 EGGS+NSE

Input: \mathbf{X} , k , \mathcal{F} , Θ , \mathcal{T} , \hat{n} .

- 1: Select \hat{n} landmarks from \mathbf{X} by k-means or randomly to form $\hat{\mathbf{X}}$.
- 2: Apply Algorithm 1 to $\hat{\mathbf{X}}$ and get $\hat{\mathbf{Z}}$.
- 3: Use mini-batch Adam to solve (27).
- 4: Compute \mathbf{Z} by (28).
- 5: Perform k-means on \mathbf{Z} .

Output: k clusters: C_1, \dots, C_k .

V. EXPERIMENTS

In this paper, we test the proposed method on the following benchmark image datasets: Extended Yale B Face [15], ORL Face [34], COIL20 [28], AR Face [24], MNIST [16], Fashion-MNIST [42], and GTSRB [38]. Details about the datasets are in the appendix. All algorithms and experiments are conducted in MATLAB on a MacBook Pro with 2.3 GHz Intel i5 Core and 8GB RAM.

A. Performance on small datasets

We first compare our method EGGS with SSC [5], LRR [21], EDSC [29]⁵, KSSC [31], SSC-OMP [45], BDR-Z [22], and BDR-B [22]. The parameter λ in each of SSC, LRR, and KSSC is chosen from $\{0.01, 0.02, 0.05, 0.1, 0.2, 0.3, 0.4, 0.5\}$.

⁵It's an improved version of LSR [23]. The original LSR and its kernel version have low accuracy [22] and hence are not compared in this paper.

The λ in BDR is chosen from $\{5, 10, 20, \dots, 80\}$. The γ in BDR-B and BDR-Z is chosen from $\{0.01, 0.1, 1\}$. The parameter s in SSC-OMP is chosen from $\{3, 4, \dots, 15\}$. We report the results of these methods with their best hyper parameters. In EGGS, we set $\Theta = \{0.01, 0.1, 1\}$ and $\mathcal{T} = \{5, 6, \dots, 15\}$.

We randomly select 5, 10 and 20 subjects from the Yale B dataset to test the proposed method EGGS in comparison with the six baseline methods. The mean, median, and standard deviation of 20 trials as well as the average time cost are reported in Table I. We see that the mean and median clustering accuracies of EGGS are higher than those of other methods in all cases. The standard deviation of EGGS is also lower than other methods in most cases. SSC-OMP is faster than EGGS. Notice if we implement Algorithm 1 parallelly, the time cost of EGGS can be reduced significantly (at most 1/6 of the current cost). These results verified that the proposed EGGS is more accurate, stable, and efficient than the compared methods.

Since the original MNIST and Fashion-MNIST datasets are too large for SSC, LRR, KSSC, and BDR, here we use a small subset of 1000 samples by randomly selecting 100 images from every class. The clustering accuracy and time cost on the six datasets are reported in Table II. On Yale B and ORL datasets, EGGS outperformed other methods significantly. SSC and KSSC have high clustering accuracy on COIL20. The reason is that the different poses of the images can be well recognized and exploited by the sparse self-expressive models in SSC and KSSC. On MNIST1k, the difference among SSC, KSSC, BDR, and EGGS are not significant. SSC-OMP and EGGS are more efficient than other methods. The clustering accuracy of EGGS is higher than that of SSC-OMP in every case.

It is worth mentioning that the search space of EGGS can be arbitrarily large and the performance of EGGS is stable. For example, when $\Theta = \{10^{-8}, 10^{-7}, \dots, 10^8\}$ and $\mathcal{T} = \{3, 4, \dots, 100\}$, the clustering accuracy of EGGS on Yale B is still 0.897. See Section 2.3 of the supplement. But we use a relatively compact search space to avoid the highly unnecessary computation.

Actually, REG is also valid for other methods such as SSC. By incorporating SSC and KSSC into EGGS, the clustering accuracy on COIL20 can be improved to 0.918 from 0.782. But there is no improvement on other datasets. The computational cost increased significantly because SSC and KSSC has no closed-form solution.

B. Performance on large datasets

We compare our EGGS+NSE (Algorithm 2) with LSC-K [3], SSSC [33], SSC-OMP [45], and S⁵C [25], and S³COMP-C [4], on MNIST and Fashion-MNIST. Two subsets consisting of 10,000 samples are also considered. The parameter settings as well as more results are in the supplementary material. The clustering accuracy and standard deviation of 10 repeated trials are reported in Table III. We see that the clustering accuracies of SSC-OMP and SSSC are much lower than other methods in all cases. Our EGGS+NSE has highest clustering accuracy in every case. Then improvement of EGGS+NSE on MNIST is 13.5% over the second best method LSC-K. Moreover, EGGS+NSE is always more efficient than other methods.

TABLE I

CLUSTERING ACCURACY AND TIME COST (SECOND) ON THE SUBSETS OF THE EXTENDED YALE FACE B DATABASE. THE BEST TWO VALUES IN EACH CASE ARE HIGHLIGHTED IN BOLD FONT. THE TIME COST OF EGGS CAN BE REDUCED SIGNIFICANTLY IF ALGORITHM 1 IS IMPLEMENTED PARALLELLY.

		SSC	LRR	EDSC	KSSC	SSC-OMP	BDR-Z	BDR-B	EGGS
5 subjects	mean	0.883	0.932	0.967	0.880	0.952	0.908	0.964	0.972
	median	0.901	0.926	0.979	0.930	0.972	0.973	0.984	0.984
	std	0.089	0.032	0.044	0.100	0.057	0.125	0.061	0.038
	time	2.7	7.3	0.6	2.1	0.3	1.2	1.2	0.8
10 subjects	mean	0.841	0.875	0.945	0.798	0.859	0.777	0.924	0.969
	median	0.859	0.874	0.959	0.788	0.833	0.714	0.961	0.969
	std	0.066	0.032	0.036	0.074	0.057	0.103	0.085	0.017
	time	9.5	33.0	2.4	12.4	0.5	7.6	7.6	1.6
20 subjects	mean	0.779	0.799	0.881	0.736	0.814	0.664	0.781	0.911
	median	0.780	0.814	0.887	0.747	0.812	0.672	0.788	0.903
	std	0.063	0.041	0.059	0.077	0.037	0.045	0.060	0.035
	time	54.9	158.3	13.5	86.1	2.1	63.2	63.2	5.0

TABLE II

CLUSTERING ACCURACY AND TIME COST (SECOND) ON THE 6 DATASETS. AS SSC-OMP AND EGGS ARE MORE EFFICIENT THAN OTHER METHODS, WE PERFORM THEM FOR 20 TIMES AND REPORT THE MEAN VALUES AND STANDARD DEVIATIONS. FOR THE MNIST1K, WE REPORT THE AVERAGE RESULTS OF 20 TRIALS BECAUSE THE SUBSET IS FORMED RANDOMLY. EGGS CHOSE LINEAR REGRESSION FOR YALE B AND AR AND CHOSE KERNEL REGRESSION FOR OTHER DATASETS.

		SSC	LRR	EDSC	KSSC	SSC-OMP	BDR-Z	BDR-B	EGGS
Yale B	acc	0.723	0.643	0.806	0.649	0.768 (0.015)	0.596	0.719	0.897 (0.01)
	time	273.8	928.1	58.6	464.3	8.9	368.8	368.8	19.1
ORL	acc	0.711	0.762	0.712	0.707	0.665 (0.022)	0.739	0.735	0.795 (0.011)
	time	2.7	8.8	2.0	2.6	0.4	3.9	3.9	2.3
COIL20	acc	0.871	0.729	0.759	0.912	0.658 (0.030)	0.713	0.791	0.782 (0.012)
	time	61.8	221.2	15.4	100.6	2.5	86.8	86.8	7.6
AR	acc	0.718	0.769	0.673	0.726	0.669 (0.022)	0.745	0.751	0.786 (0.013)
	time	317.5	1220.6	69.1	627.4	57.6	578.7	578.7	43.4
MNIST-1k	acc	0.596 (0.054)	0.513 (0.037)	0.536 (0.035)	0.577 (0.053)	0.542 (0.038)	0.576 (0.037)	0.578 (0.043)	0.615 (0.041)
	time	24.9	69.1	5.2	32.8	1.3	26.9	26.9	2.5
Fashion-MNIST-1k	acc	0.553 (0.025)	0.515 (0.014)	0.544 (0.017)	0.548 (0.016)	0.566 (0.034)	0.574 (0.019)	0.563 (0.031)	0.581 (0.025)
	time	24.1	68.5	5.1	35.9	1.2	25.7	25.7	2.6

In addition to performing clustering on the raw pixels of the images, here, for MNIST (also Fashion-MNIST), following the same procedures of [4], we compute a feature vector of dimension 3,472 using the scattering convolution network [1] and then reduce the dimension to 500 using PCA. The clustering is performed on the $500 \times 70,000$ data. Following [4], we also consider the GTSR dataset [38] consisting of 12,390 images of street signs in 14 categories, extract a 1568-dimensional HOG feature, and reduce the dimension to 500 by PCA. The results are reported in Table IV. Our method EGGS+NSE outperformed other methods. Note that the clustering accuracy of the deep learning method proposed in [47] on MNIST and Fashion-MNIST are 0.9409 and 0.7214 respectively. So our method outperformed the deep learning method only on MNIST, but the deep learning method has very high computational cost. One observation is that, for Fashion-MNIST, the feature extraction by scattering convolution network provided limited improvement in clustering.

VI. CONCLUSION

In this paper, we have proposed a novel clustering method called EGGS. The automatic model and hyper-parameter searching and high efficiency of EGGS provide us huge convenience and stability in real applications. We also provide a neural sparse embedding method to extend EGGS to large-scale datasets. Extensive experiments showed the effectiveness and superiority of our methods over baseline methods.

On the other hand, in EGGS, it will be helpful to enlarge the search space \mathbb{S} to improve the clustering accuracy. For instance, we may include more affinity-matrix-construction methods (e.g. KSSC and deep learning) in \mathcal{F} . EGGS can be a baseline method or a convenient tool to evaluate different models and hyper parameters in clustering problems.

APPENDIX

A. Proof for claims and theorems

1) Proof for Claim 1:

TABLE III

CLUSTERING ACCURACY (MEAN VALUE AND STANDARD DEVIATION) AND TIME COST (SECOND) ON MNIST AND FASHION MNIST. THE TIME COST OF S³COMP IS DIVIDED BY 20 (THE PARAMETER T IN [4]) BECAUSE WE HAVEN'T USED THE PARALLEL ALGORITHM OF THE METHOD (LIMITED BY THE RAM). “—” MEANS THE COMPUTATION IS OUT OF MEMORY.

		LSC-K[3]	SSSC[33]	SSC-OMP[45]	S ⁵ C[25]	S ³ COMP-C[4]	EGGS+NSE
MNIST-10k	acc	0.652(0.037)	0.529(0.031)	0.431(0.014)	0.646(0.045)	0.623(0.028)	0.687(0.035)
	time	18.9	31.2	26.4	82.3	710.4/20	16.2
MNIST	acc	0.665(0.021)	0.548(0.025)	0.453(0.017)	0.627(0.025)	—	0.755(0.022)
	time	329.2	97.8	1178.3	961.5	—	86.9
Fashion-MNIST-10k	acc	0.571(0.025)	0.537(0.016)	0.509(0.038)	0.565(0.021)	0.569(0.024)	0.576(0.011)
	time	18.6	29.1	26.8	107.3	707.2/20	17.3
Fashion-MNIST	acc	0.561(0.015)	0.528(0.013)	0.359(0.017)	0.559(0.013)	—	0.586(0.008)
	time	335.1	94.6	1156.6	932.6	—	88.7

TABLE IV

CLUSTERING ACCURACY (MEAN VALUE AND STANDARD DEVIATION) AND TIME COST (SECOND) ON MNIST AND FASHION-MNIST WITH FEATURE EXTRACTION. “—” MEANS THE COMPUTATION IS OUT OF MEMORY AND “/” MEANS THE ALGORITHM WAS PERFORMED ON A COMPUTATIONAL PLATFORM NOT COMPARABLE TO OURS. THE UNDERLINED VALUES ARE FROM [4].

		LSC-K[3]	SSSC[33]	SSC-OMP[45]	S ⁵ C[25]	S ³ COMP-C[4]	EGGS+NSE
MNIST	acc	0.8659(0.0215)	0.8229(0.0503)	<u>0.8159</u>	0.7829(0.0283)	<u>0.9632</u>	0.9775(0.0034)
	time	273.6	83.3	<u>280.6</u>	907.5	<u>416.8</u>	59.2
Fashion-MNIST	acc	0.6131(0.0298)	0.6220(0.0159)	0.3796(0.0217)	0.6057(0.0227)	—	0.6398(0.0133)
	time	251.8	71.64	1013.9	913.2	—	61.9
GTSRB	acc	0.8711(0.0510)	0.8101(0.0321)	<u>0.8252</u>	0.9044(0.0267)	<u>0.9554</u>	0.9873(0.0126)
	time	31.2	37.1	/	98.7	/	16.8

Proof. The stochastic transition matrix of G is defined as

$$\mathbf{P} = \mathbf{D}^{-1}\mathbf{A}. \quad (29)$$

In [26], it was showed that

$$\text{MNCut}(\mathcal{C}) \geq k - \sum_{i=1}^k \varrho_i(\mathbf{P}), \quad (30)$$

where $\varrho_i(\mathbf{P})$ denotes the i -th largest eigenvalue of \mathbf{P} and $1 = \varrho_1(\mathbf{P}) \geq \varrho_2(\mathbf{P}) \geq \dots \geq \varrho_k(\mathbf{P})$. According to Lemma 3 of [26], we have

$$\sigma_i(\mathbf{L}) = 1 - \varrho_i(\mathbf{P}), \quad \forall i = 1, \dots, n. \quad (31)$$

Substituting (31) into (30), we have

$$\text{MNCut}(\mathcal{C}) \geq \sum_{i=1}^k \sigma_i(\mathbf{L}). \quad (32)$$

□

Remark 1. \mathcal{C} can be any partition of the nodes of G . Let \mathcal{C}^* be the optimal partition. Then $\text{MNCut}(\mathcal{C}^*) = \sum_{i=1}^k \sigma_i(\mathbf{L})$. If $\sum_{i=1}^k \sigma_i(\mathbf{L}) = 0$, there are no connections (edges) among C_1^*, \dots, C_k^* .

2) *Proof for Claim 2:*

Proof. For $i = 1, \dots, k$, we aim to partition C_i into two subsets, denoted by C_i^1 and C_i^2 . Then we define

$$\text{MNCut}(C_i) = \frac{\text{Cut}(C_i^1, C_i^2)}{\text{Vol}(C_i^1)} + \frac{\text{Cut}(C_i^2, C_i^1)}{\text{Vol}(C_i^2)}. \quad (33)$$

It follows that

$$\text{MNCut}(C_i) \geq \sum_{j=1}^2 \sigma_j(\mathbf{L}_{C_i}) \geq \sigma_2(\mathbf{L}_{C_i}) = \text{ac}(C_i), \quad (34)$$

where \mathbf{L}_{C_i} denotes the Laplacian matrix of C_i an $i = 1, \dots, k$. Since $\sigma_{k+1}(\mathbf{L}) = \min\{\text{ac}(C_1), \dots, \text{ac}(C_k)\}$, we have

$$\min_{1 \leq i \leq k} \text{MNCut}(C_i) \geq \sigma_{k+1}(\mathbf{L}). \quad (35)$$

Therefore, $\sigma_{k+1}(\mathbf{L})$ measures the least connectivity of C_1, \dots, C_k . This finished the proof. □

Remark 2. When $\sigma_{k+1}(\mathbf{L})$ is large, the connectivity in each of C_1, \dots, C_k is strong. Otherwise, the connectivity in each of C_1, \dots, C_k is weak. When $\sigma_{k+1}(\mathbf{L}) = 0$, at least one of C_1, \dots, C_k contains at least two components, which means the nodes of G can be partitioned into $k+1$ or more clusters.

3) *Proof for Theorem 1:*

Proof. According to Theorem 1 of [27], we have

$$\text{dist}(\mathcal{C}, \mathcal{C}') < \frac{3\delta}{\sigma_{k+1}(\mathbf{L}) - \sigma_k(\mathbf{L})}. \quad (36)$$

Since $\text{reg}(\mathbf{L}) = \frac{\sigma_{k+1}(\mathbf{L}) - \frac{1}{k} \sum_{i=1}^k \sigma_i(\mathbf{L})}{\frac{1}{k} \sum_{i=1}^k \sigma_i(\mathbf{L}) + \epsilon}$, we have

$$\sigma_{k+1}(\mathbf{L}) - \sigma_k(\mathbf{L}) = \text{reg}(\mathbf{L})(\bar{\sigma} + \epsilon) + \bar{\sigma} - \sigma_k(\mathbf{L}), \quad (37)$$

where $\bar{\sigma} = \frac{1}{k} \sum_{i=1}^k \sigma_i(\mathbf{L}) \geq \epsilon$. Invoking (37) into (36), we arrive at

$$\begin{aligned} \text{dist}(\mathcal{C}, \mathcal{C}') &< \frac{3\delta}{\text{reg}(\mathbf{L})(\bar{\sigma} + \epsilon) + \bar{\sigma} - \sigma_k(\mathbf{L})} \\ &\leq \frac{3\delta}{2\epsilon\text{reg}(\mathbf{L}) + \bar{\sigma} - k\bar{\sigma}} \\ &\leq \frac{3\delta}{2\epsilon\text{reg}(\mathbf{L}) + (1-k)\eta\epsilon} \\ &\leq \frac{1.5\delta\epsilon^{-1}}{\text{reg}(\mathbf{L}) + (1-k)\eta/2}. \end{aligned}$$

This finished the proof. \square

4) Proof for Proposition 2:

Proof. Since $\hat{\mathbf{c}}$ is the optimal solution, we have

$$\begin{aligned}\phi(\mathbf{x}_i)^\top (\phi(\mathbf{y}) - \phi(\mathbf{X})\hat{\mathbf{c}}) + \lambda\hat{c}_i &= 0, \\ \phi(\mathbf{x}_j)^\top (\phi(\mathbf{y}) - \phi(\mathbf{X})\hat{\mathbf{c}}) + \lambda\hat{c}_j &= 0.\end{aligned}$$

It follows that

$$\begin{aligned}\|\hat{c}_i - \hat{c}_j\| &= \|(\phi(\mathbf{x}_i) - \phi(\mathbf{x}_j))^\top (\phi(\mathbf{y}) - \phi(\mathbf{X})\hat{\mathbf{c}})\| \\ &\leq \|\phi(\mathbf{x}_i) - \phi(\mathbf{x}_j)\| \|\phi(\mathbf{y}) - \phi(\mathbf{X})\hat{\mathbf{c}}\| \\ &= \sqrt{k(\mathbf{x}_i, \mathbf{x}_i) - 2k(\mathbf{x}_i, \mathbf{x}_j) + k(\mathbf{x}_j, \mathbf{x}_j)} \\ &\quad \times \|\phi(\mathbf{y}) - \phi(\mathbf{X})\hat{\mathbf{c}}\| \\ &= \sqrt{2 - 2k(\mathbf{x}_i, \mathbf{x}_j)} \|\phi(\mathbf{y}) - \phi(\mathbf{X})\hat{\mathbf{c}}\| \\ &\leq \sqrt{2 - 2k(\mathbf{x}_i, \mathbf{x}_j)} \|\phi(\mathbf{y})\| \\ &= \sqrt{2 - 2\exp\left(-\frac{\|\mathbf{x}_i - \mathbf{x}_j\|^2}{2\varsigma^2}\right)}.\end{aligned}\tag{38}$$

In the second and last equalities, we used the fact that $\|\phi(\mathbf{y})\| = \|\phi(\mathbf{x})\| = 1$. In the second inequality, we used the fact that $\frac{1}{2}\|\phi(\mathbf{y}) - \phi(\mathbf{X})\hat{\mathbf{c}}\|^2 + \frac{\lambda}{2}\|\hat{\mathbf{c}}\|^2 \leq \frac{1}{2}\|\phi(\mathbf{y}) - \phi(\mathbf{X})\mathbf{0}\|^2 + \frac{\lambda}{2}\|\mathbf{0}\|^2 = \frac{1}{2}\|\phi(\mathbf{y})\|^2$ because $\hat{\mathbf{c}}$ is the optimal solution. \square

5) Proof for Proposition 3:

Proof. We only need to provide an example of $\mathbf{W}_1 \in \mathbb{R}^{d \times m}$, $\mathbf{W}_2 \in \mathbb{R}^{k \times d}$, $\mathbf{b}_1 \in \mathbb{R}^d$, and $\mathbf{b}_2 \in \mathbb{R}^k$, where $d = k\mathfrak{d}$, such that the clusters can be recognized by k-means.

We organize the rows of \mathbf{W}_1 into k groups: $\mathbf{W}_1^j \in \mathbb{R}^{d \times m}$, $j = 1, \dots, k$. Let $\mathbf{W}_1^j = \mathbf{U}^{j\top}$, $j = 1, \dots, k$. Let $\mathbf{W}_1 \mathbf{x}_i = \boldsymbol{\alpha}_i = (\alpha_i^1, \dots, \alpha_i^d)$. When $\mathbf{x}_i \in \mathcal{S}_j$, we have

$$\boldsymbol{\alpha}_i^j = \mathbf{U}^{j\top} \mathbf{x}_i = \mathbf{U}^{j\top} \mathbf{U}^j \mathbf{v}_i = \mathbf{v}_i.\tag{39}$$

It follows from the assumption that

$$\max_p \alpha_{pi}^j > \mu.\tag{40}$$

Let $\mathbf{b}_1 = [b_1^1; \dots; b_1^k] = -\mu\mathbf{1}$. Then $\mathbf{h}_i^j = \text{ReLU}(\boldsymbol{\alpha}_i^j + \mathbf{b}_1^j)$ has at least one positive element. On the other hand, since

$$\boldsymbol{\alpha}_i^l = \mathbf{U}^{l\top} \mathbf{x}_i = \mathbf{U}^{l\top} \mathbf{U}^j \mathbf{v}_i \quad l \neq j,\tag{41}$$

using the assumption of μ , we have

$$|\alpha_{pi}^l| = |\mathbf{U}_{:p}^l \mathbf{U}^j \mathbf{v}_i| \leq \|\mathbf{U}_{:p}^l \mathbf{U}^j\| \|\mathbf{v}_i\| \leq \mu,\tag{42}$$

where we have used the fact $\|\mathbf{v}_i\| = 1$ because $\|\mathbf{x}_i\| = 1$. It follows that

$$\mathbf{h}_i^l = \text{ReLU}(\boldsymbol{\alpha}_i^l + \mathbf{b}_1^l) = \mathbf{0}, \quad l \neq j.$$

Now we formulate \mathbf{W}_2 as

$$\mathbf{W}_2 = \begin{bmatrix} \mathbf{q}_{11} & \mathbf{q}_{12} & \dots & \mathbf{q}_{1k} \\ \mathbf{q}_{21} & \mathbf{q}_{22} & \dots & \mathbf{q}_{2k} \\ \vdots & \vdots & \ddots & \vdots \\ \mathbf{q}_{k1} & \mathbf{q}_{k2} & \dots & \mathbf{q}_{kk} \end{bmatrix},\tag{43}$$

where $\mathbf{q}_{lj} \in \mathbb{R}^{1 \times \mathfrak{d}}$, $l, j = 1, \dots, k$. We have

$$z_{ji} = \mathbf{q}_{j1} \mathbf{h}_i^1 + \mathbf{q}_{j2} \mathbf{h}_i^2 + \dots + \mathbf{q}_{jk} \mathbf{h}_i^k = \mathbf{q}_{jj} \mathbf{h}_i^j.$$

and

$$z_{li} = \mathbf{q}_{l1} \mathbf{h}_i^1 + \mathbf{q}_{l2} \mathbf{h}_i^2 + \dots + \mathbf{q}_{lk} \mathbf{h}_i^k = \mathbf{q}_{lj} \mathbf{h}_i^j.$$

Here we have let $\mathbf{b}_2 = \mathbf{0}$. Let $\mathbf{q}_{jj} \geq \mathbf{0}$ and $\mathbf{q}_{lj} = \mathbf{0}$, we have

$$z_{ji} > z_{li} = 0.$$

Therefore, if $\mathbf{x}_i \in \mathcal{S}_j$, we have $z_{ji} > 0$ and $z_{li} = 0 \ \forall 1 \leq j \neq l \leq k$. Now performing k-means on $\mathbf{Z} = [z_1, \dots, z_n]$ can identify the clusters trivially. \square

B. More about the experiments

1) *Dataset description:* The description for the benchmark image datasets considered in this paper are as follows.

- Extended Yale B Face [15] (Yale B for short): face images (192×168) of 38 subjects. Each subject has about 64 images under various illumination conditions. We resize the images into 32×32 .
- ORL Face [34]: face images (112×92) of 40 subjects. Each subject has 10 images with different poses and facial expressions. We resize the images into 32×32 .
- COIL20 [28]: images (32×32) of 20 objects. Each object has 72 images of different poses.
- AR Face [24]: face images (165×120) of 50 males and 50 females. Each subject has 26 images with different facial expressions, illumination conditions, and occlusions. We resize the images into 42×30 .
- MNIST [16]: 70,000 grey images (28×28) of handwritten digits 0 – 9.
- Fashion-MNIST [42]: 70,000 gray images (28×28) of 10 types of fashion product.

2) *The stability of EGGS:* Though we have used a relatively compact search space in EGGS to reduce the highly unnecessary computational cost, the search space can be arbitrarily large. Figure 3 shows the clustering accuracy and the corresponding relative-eigen-gap. We can see that the region with highest relative-eigen-gap is in accordance with the region with highest clustering accuracy.

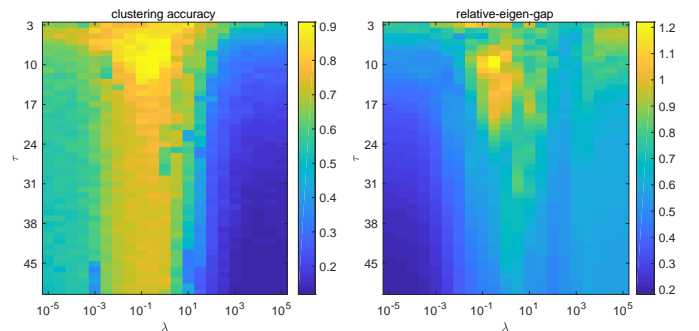


Fig. 3. Visualization of the clustering accuracy and the corresponding relative-eigen-gap when a large search space is used.

3) *Eigen-Gap versus relative-eigen-gap*: In the paper, we use relative-eigen-gap (reg) defined by (11) in the main paper because the eigen-gap (eg) rely on the scale of the small eigenvalues, which are sensitive to noise and may change significantly when using different values of \mathcal{F} , Θ , and \mathcal{T} . Table V shows the relative-eigen-gap we defined can provide much higher clustering accuracy, compared to the ordinary eigen-gap.

TABLE V
THE COMPARISON OF EGGS WITH EIGEN-GAP AND EGGS WITH
RELATIVE-EIGEN-GAP

	YaleB	ORL	COIL20	AR	MNIST	F-MNIST
eg	0.790	0.768	0.619	0.775	0.663	0.562
reg	0.897	0.795	0.782	0.786	0.755	0.595

4) *Hyper-parameter settings of large-scale clustering methods*: On MNIST-10k, MNIST, Fashion-MNIST-10k, and Fashion-MNIST, the parameter settings of [3], SSSC [33], SSC-OMP [45], and S⁵C [25], and S³COMP-C [4], and EGGS+NSE are shown in Table VI. These hyper parameters have been determined via grid search and the best (as possible) values are used.

TABLE VI
HYPER-PARAMETER SETTINGS OF THE COMPARED METHODS ON
MNIST-10K, MNIST, FASHION-MNIST-10K, AND FASHION-MNIST. s
DENOTES THE NUMBER OF LANDMARK DATA POINTS. IN THE
OPTIMIZATION (MINI-BATCH ADAM) OF EGGS+NSE, THE EPOCH
NUMBER, BATCH SIZE, AND STEP SIZE ARE 200, 128, AND 10^{-3}
RESPECTIVELY.

LSC-K	$s = 1000, r = 3$
SSSC	$s = 1000, \lambda = 0.01$
SSC-OMP	$K = 10$ (sparsity)
S ⁵ C	$s = 1000, \lambda = 0.1$ or 0.2
S ³ COMP-C	$T = 20, \lambda = 0.4, \delta = 0.9$
EGGS+NSE	$s = 1000, d = 200, \gamma = 10^{-5}$

5) *Influence of hyper-parameters in EGGS+NSE*: We investigate the effects of the type of activation function and the number (d) of nodes in the hidden layer of NSE. For convenience, we used a fixed random seed of MATLAB (rng(1)). Figure 4 shows the clustering accuracy on MNIST given by EGGS+NSE with different activation function and different d . We see that ReLU outperformed tanh consistently. The reason is that the nonlinear mapping g from the data space to the nullspace of the Laplacian matrix is nonsmooth and ReLU is more effective than tanh in approximating nonsmooth functions. In addition, when d increases, the clustering accuracy of EGGS+NSE with ReLU often becomes higher because wider network often has higher ability of function approximation.

Figure 5 shows the clustering accuracy on MNIST given by EGGS+NSE with different γ and α . When α is too small (say 10^{-4} , the clustering accuracy is low, because the training error is quite large in 200 epochs. In fact, by increasing the training epochs, the clustering accuracy can be improved, which however will increase the time cost. When α is relatively large, the clustering accuracy is often higher than 0.755. On the other hand, EGGS+NSE is not sensitive to γ provided that it is not too large.

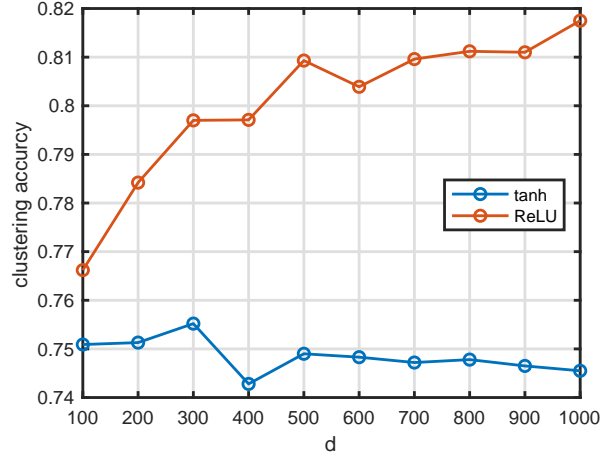


Fig. 4. ReLU v.s. tanh (hyperbolic tangent) in the hidden layer of EGGS+NSE on MNIST. When using ReLU, we set $\gamma = 10^{-5}$ and $\alpha = 10^{-3}$ (the step size in Adam). When using tanh, we set $\gamma = 10^{-3}$ and $\alpha = 10^{-2}$, which perform best in this case. Notice that the clustering accuracy when using ReLU is higher than 0.78 in almost all cases, which is higher than the value (say 0.755) we reported in the main paper. The reason is than in the main paper, we reported the mean value of 10 repeated trials but here we reports the value of a single trial.

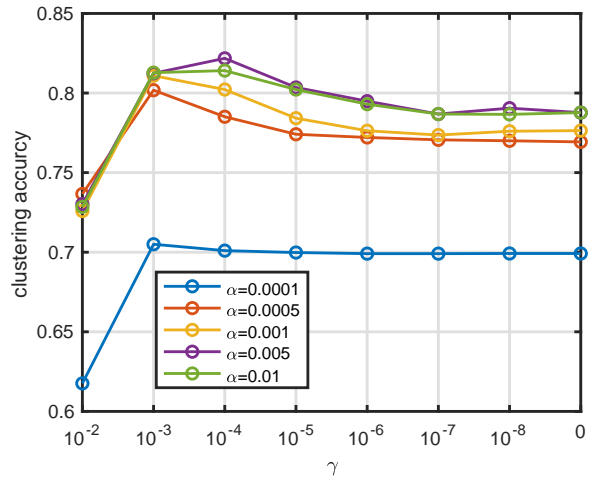


Fig. 5. Influence of γ and α in EGGS+NSE on MNIST. We set $d = 200$ and use ReLU.

Figure 6 shows the mean value and standard deviation (10 repeated trials) of the clustering accuracy on MNIST given by EGGS+NSE with different number (denoted by s) of landmark points. It can be found that when the s increases, the clustering accuracy increases and its standard deviation becomes smaller. When s is large enough, the improvement is not significant.

REFERENCES

- [1] Joan Bruna and Stéphane Mallat. Invariant scattering convolution networks. *IEEE transactions on pattern analysis and machine intelligence*, 35(8):1872–1886, 2013.
- [2] Deng Cai and Xinlei Chen. Large scale spectral clustering via landmark-based sparse representation. *IEEE transactions on cybernetics*, 45(8):1669–1680, 2014.
- [3] Xinlei Chen and Deng Cai. Large scale spectral clustering with landmark-based representation. In *Twenty-fifth AAAI conference on artificial intelligence*. Citeseer, 2011.

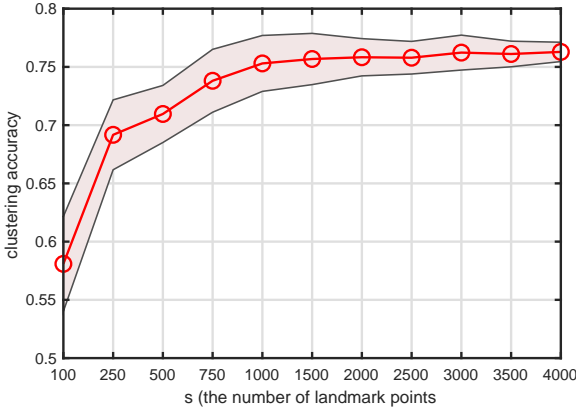


Fig. 6. Influence of the number of landmark points in EGGS+NSE on MNIST. We set $d = 200$, $\gamma = 10^{-5}$, and $\alpha = 10^{-3}$. The shadow denotes the standard deviation of 10 trials.

- [4] Ying Chen, Chun-Guang Li, and Chong You. Stochastic sparse subspace clustering. In *Proceedings of the IEEE/CVF Conference on Computer Vision and Pattern Recognition*, pages 4155–4164, 2020.
- [5] E. Elhamifar and R. Vidal. Sparse subspace clustering: Algorithm, theory, and applications. *IEEE Transactions on Pattern Analysis and Machine Intelligence*, 35(11):2765–2781, 2013.
- [6] Miroslav Fiedler. Algebraic connectivity of graphs. *Czechoslovak mathematical journal*, 23(2):298–305, 1973.
- [7] N. Halko, P. G. Martinsson, and J. A. Tropp. Finding structure with randomness: Probabilistic algorithms for constructing approximate matrix decompositions. *SIAM Review*, 53(2):217–288, 2011.
- [8] Harold V Henderson and Shayle R Searle. On deriving the inverse of a sum of matrices. *SIAM Review*, 23(1):53–60, 1981.
- [9] Juhua Hu, Qi Qian, Jian Pei, Rong Jin, and Shenghuo Zhu. Finding multiple stable clusterings. *Knowledge and Information Systems*, 51(3):991–1021, 2017.
- [10] Pan Ji, Mathieu Salzmann, and Hongdong Li. Shape interaction matrix revisited and robustified: Efficient subspace clustering with corrupted and incomplete data. In *Proceedings of the IEEE International Conference on Computer Vision (ICCV)*, December 2015.
- [11] Pan Ji, Tong Zhang, Hongdong Li, Mathieu Salzmann, and Ian Reid. Deep subspace clustering networks. In *Advances in Neural Information Processing Systems*, pages 24–33, 2017.
- [12] Zhao Kang, Zhiping Lin, Xiaofeng Zhu, and Wenbo Xu. Structured graph learning for scalable subspace clustering: From single view to multiview. *IEEE Transactions on Cybernetics*, pages 1–11, 2021.
- [13] Mohsen Kheirandishfard, Fariba Zohrizadeh, and Farhad Kamangar. Deep low-rank subspace clustering. In *Proceedings of the IEEE/CVF Conference on Computer Vision and Pattern Recognition (CVPR) Workshops*, June 2020.
- [14] Diederik P Kingma and Jimmy Ba. Adam: A method for stochastic optimization. *arXiv preprint arXiv:1412.6980*, 2014.
- [15] Lee Kuang-Chih, J. Ho, and D. J. Kriegman. Acquiring linear subspaces for face recognition under variable lighting. *IEEE Transactions on Pattern Analysis and Machine Intelligence*, 27(5):684–698, 2005.
- [16] Yann LeCun, Léon Bottou, Yoshua Bengio, and Patrick Haffner. Gradient-based learning applied to document recognition. *Proceedings of the IEEE*, 86(11):2278–2324, 1998.
- [17] Chun-Guang Li and Rene Vidal. Structured sparse subspace clustering: A unified optimization framework. In *Proceedings of the IEEE conference on computer vision and pattern recognition*, pages 277–286, 2015.
- [18] Chun-Guang Li and Rene Vidal. A structured sparse plus structured low-rank framework for subspace clustering and completion. *IEEE Transactions on Signal Processing*, 64(24):6557–6570, 2016.
- [19] Jun Li, Hongfu Liu, Zhiqiang Tao, Handong Zhao, and Yun Fu. Learnable subspace clustering. *arXiv preprint arXiv:2004.04520*, 2020.
- [20] Jun Li and Handong Zhao. Large-scale subspace clustering by fast regression coding. In *IJCAI*, 2017.
- [21] G. Liu, Z. Lin, S. Yan, J. Sun, Y. Yu, and Y. Ma. Robust recovery of subspace structures by low-rank representation. *IEEE Transactions on Pattern Analysis and Machine Intelligence*, 35(1):171–184, 2013.
- [22] Canyi Lu, Jiashi Feng, Zhouchen Lin, Tao Mei, and Shuicheng Yan. Subspace clustering by block diagonal representation. *IEEE transactions on pattern analysis and machine intelligence*, 41(2):487–501, 2018.

- [23] Can-Yi Lu, Hai Min, Zhong-Qiu Zhao, Lin Zhu, De-Shuang Huang, and Shuicheng Yan. Robust and efficient subspace segmentation via least squares regression. In *European conference on computer vision*, pages 347–360. Springer, 2012.
- [24] Aleix M Martínez and Avinash C Kak. PCA versus LDA. *IEEE transactions on pattern analysis and machine intelligence*, 23(2):228–233, 2001.
- [25] Shin Matsushima and Maria Brbic. Selective sampling-based scalable sparse subspace clustering. In *Advances in Neural Information Processing Systems*, pages 12416–12425, 2019.
- [26] Marina Meila. The multicut lemma. *UW Statistics Technical Report*, 417, 2001.
- [27] Marian Meila, Susan Shortreed, and Liang Xu. Regularized spectral learning. In *AISTATS*. PMLR, 2005.
- [28] S. A. Nene, S. K. Nayar, and H. Murase. Columbia object image library (coil-20). Report, Columbia University, 1996.
- [29] Pan Ji, M. Salzmann, and Hongdong Li. Efficient dense subspace clustering. In *IEEE Winter Conference on Applications of Computer Vision*, pages 461–468, 2014.
- [30] V. M. Patel, Nguyen Hien Van, and R. Vidal. Latent space sparse and low-rank subspace clustering. *Selected Topics in Signal Processing, IEEE Journal of*, 9(4):691–701, 2015.
- [31] V. M. Patel and R. Vidal. Kernel sparse subspace clustering. In *2014 IEEE International Conference on Image Processing (ICIP)*, pages 2849–2853, Oct 2014.
- [32] Xi Peng, Huajin Tang, Lei Zhang, Zhang Yi, and Shijie Xiao. A unified framework for representation-based subspace clustering of out-of-sample and large-scale data. *IEEE transactions on neural networks and learning systems*, 27(12):2499–2512, 2015.
- [33] Xi Peng, Lei Zhang, and Zhang Yi. Scalable sparse subspace clustering. In *Proceedings of the IEEE conference on computer vision and pattern recognition*, pages 430–437, 2013.
- [34] F. S. Samaria and A. C. Harter. Parameterisation of a stochastic model for human face identification. In *Proceedings of 1994 IEEE Workshop on Applications of Computer Vision*, pages 138–142, Dec 1994.
- [35] Junghoon Seo, Jamyoung Koo, and Taegyun Jeon. Deep closed-form subspace clustering. In *Proceedings of the IEEE International Conference on Computer Vision Workshops*, pages 0–0, 2019.
- [36] Jie Shen and Ping Li. Learning structured low-rank representation via matrix factorization. In *Proceedings of the 19th International Conference on Artificial Intelligence and Statistics*, volume 51 of *Proceedings of Machine Learning Research*, pages 500–509, Cadiz, Spain, 09–11 May 2016. PMLR.
- [37] Sho Sonoda and Noboru Murata. Neural network with unbounded activation functions is universal approximator. *Applied and Computational Harmonic Analysis*, 43(2):233 – 268, 2017.
- [38] Johannes Stalkamp, Marc Schlipsing, Jan Salmen, and Christian Igel. Man vs. computer: Benchmarking machine learning algorithms for traffic sign recognition. *Neural networks*, 32:323–332, 2012.
- [39] R. Vidal. Subspace clustering. *IEEE Signal Processing Magazine*, 28(2):52–68, 2011.
- [40] Ulrike Von Luxburg. A tutorial on spectral clustering. *Statistics and computing*, 17(4):395–416, 2007.
- [41] Shusen Wang, Bojun Tu, Congfu Xu, and Zhihua Zhang. Exact subspace clustering in linear time. In *Proceedings of the Twenty-Eighth AAAI Conference on Artificial Intelligence*, pages 2113–2120, 2014.
- [42] Han Xiao, Kashif Rasul, and Roland Vollgraf. Fashion-mnist: a novel image dataset for benchmarking machine learning algorithms, 2017.
- [43] Chong You, Chi Li, Daniel P Robinson, and René Vidal. Scalable exemplar-based subspace clustering on class-imbalanced data. In *Proceedings of the European Conference on Computer Vision (ECCV)*, pages 67–83, 2018.
- [44] Chong You, Chun-Guang Li, Daniel P Robinson, and René Vidal. Oracle based active set algorithm for scalable elastic net subspace clustering. In *Proceedings of the IEEE conference on computer vision and pattern recognition*, pages 3928–3937, 2016.
- [45] Chong You, Daniel Robinson, and René Vidal. Scalable sparse subspace clustering by orthogonal matching pursuit. In *Proceedings of the IEEE conference on computer vision and pattern recognition*, pages 3918–3927, 2016.
- [46] Junjian Zhang, Chun-Guang Li, Chong You, Xianbiao Qi, Honggang Zhang, Jun Guo, and Zhouchen Lin. Self-supervised convolutional subspace clustering network. In *Proceedings of the IEEE Conference on Computer Vision and Pattern Recognition*, pages 5473–5482, 2019.
- [47] Tong Zhang, Pan Ji, Mehrtash Harandi, Wenbing Huang, and Hongdong Li. Neural collaborative subspace clustering. In *International Conference on Machine Learning*, pages 7384–7393, 2019.